Chemical Science

ROYAL SOCIETY OF CHEMISTRY

EDGE ARTICLE

View Article Online
View Journal | View Issue

Cite this: *Chem. Sci.*, 2026, **17**, 7037

All publication charges for this article have been paid for by the Royal Society of Chemistry

Dynamic-structural-distortion of spheroidene activates a hidden $3A_g^-$ state mediating carotenoid-to-bacteriochlorophyll energy transfer in a light-harvesting 2 complex

Bo Peng,†[a] Mingqing Chen,†[b] Tengfei Ma,†[a] Yifan Huang,[b] Peng Wang *[b] and Weimin Liu *[a]

Received 3rd November 2025
Accepted 30th January 2026

DOI: 10.1039/d5sc08508j

rsc.li/chemical-science

Carotenoids extend the absorption range of photosynthesis and transfer excitation energy to (bacterio-)chlorophylls with remarkable efficiency, yet the microscopic mechanism of this process, especially the role of the S_X intermediate, remains unresolved. Here, we use femtosecond stimulated Raman spectroscopy, whose high vibrational frequency and temporal resolutions enable direct tracking of excited-state intermediates and their symmetry characteristics. By probing spheroidene in both solution and the light-harvesting 2 complex of Rhodobacter sphaeroides, we reveal structural change in the S_2 ($1B_u^+$) state that forms distorted S_X and S_1 ($2A_g^-$) intermediates. The S_X state is assigned to optically forbidden $3A_g^-$ configuration rather than the earlier $1B_u^-$ or A_g^+ proposals and is identified as an efficient pathway for energy transfer to bacteriochlorophylls. The spheroidene-to-bacteriochlorophyll energy transfer efficiencies are quantified as 32% *via* the S_X state, combined with 50% from the S_2 state and 12% from the S_1 state, yielding an overall transfer efficiency of 94%, in excellent agreement with previous reports. We propose that the observed structural distortions of spheroidene dynamically enhance coulombic coupling with surrounding bacteriochlorophylls, which may underlie the remarkably high efficiency of excitation energy transfer.

Introduction

Carotenoids are essential for photosynthesis, where they harvest solar energy and transfer it to (bacterio-)chlorophylls with remarkable efficiency.[1] Despite decades of study, the microscopic mechanisms remain elusive, particularly the role of intermediate optically forbidden states and their role in facilitating ultrafast energy transfer. The bacterial light-harvesting 2 (LH2) complex provides an ideal system to address this challenge.[2,3] In the *Rhodobacter sphaeroides* LH2 complex, ultrafast spectroscopy has shown that the spheroidene transfers excitation energy to neighboring BChls with efficiencies exceeding >90%.[4–7] However, the contribution of the S_X intermediate and the precise nature of its electronic symmetry remain controversial.[7–16] Previous experiments assigned an optically forbidden $1B_u^-$ symmetry to this S_X state;[9–12] the involvement of the optically forbidden $1B_u^-$ state reconciled with the theoretical calculation, which positions it between optically allowed S_2 ($1B_u^+$) and optically forbidden S_1 ($2A_g^-$) states for the conjugation length $N = 10$.[13–15] By contrast, other theoretical studies proposed an optically forbidden A_g^+ assignment,[16] leaving both the nature and the functional role of the S_X state unresolved. This controversy arises largely because experimentally determining the precise symmetry of the intermediate state between S_2 and S_1 remains highly challenging.

In this work, we address this challenge by employing femtosecond stimulated Raman spectroscopy (FSRS)[17,18] to investigate the real-time structural evolution of spheroidene in both solution and the intact LH2 complex extracted from *Rhodobacter sphaeroides 2.4.1*. FSRS offers distinct advantages over conventional electronic spectroscopy by simultaneously providing high temporal and spectral resolution, enabling direct observation of individual excited-state intermediates.[19] Moreover, the symmetry properties of carotenoid excited states can be disentangled *via* characteristic vibrational modes. For instance, Raman signals near 1800 cm^{-1} have been linked to C=C stretching vibronic coupling mode involving A_g^- symmetry,[17,18,20–25] while additional features reveal C=C stretching diabatic mixing between B_u^+ and A_g^- (or B_u^-) states.[13,17,26–28] These capabilities establish FSRS as a powerful tool for probing the structural and symmetry evolution of photoexcited carotenoids.

[a]*School of Physical Science and Technology, ShanghaiTech University, Shanghai 201210, China. E-mail: liuwm@shanghaitech.edu.cn*

[b]*Key Laboratory of Advanced Light Conversion Materials and Biophotonics, School of Chemistry and Life Resources, Renmin University of China, Beijing 100872, P. R. China. E-mail: wpeng_chem@ruc.edu.cn*

† These authors contributed equally to this work.

Leveraging these strengths, we discovered a functional S_X state between the S_2 ($1B_u^+$) and S_1 ($2A_g^-$) states that does not conform to the previously proposed $1B_u^-$ or A_g^+ assignments, but instead corresponds to an optically forbidden $3A_g^-$ state. This state arises from photoinduced structural distortions in the S_2 ($1B_u^+$) state, leading to formation of twisted S_X ($3A_g^-$) and S_1 ($2A_g^-$) states. Importantly, we show that the S_X state contributes 32% to excitation energy transfer to BChls, together with 50% from S_2 and 12% from S_1, yielding a total transfer efficiency of 94% in excellent agreement with previous reports.[4–7]

Methods

Sample preparation

Tris(hydroxymethyl)aminomethane (Tris) (>99%) and diethylaminoethyl cellulose (DEAE-52) were purchased from Solarbio Life Science (Beijing), inorganic salts (both A. R.) were purchased from Sinopharm Chemical Reagent Beijing Co., and lauryl dimethylamine oxide (LDAO, 30%) and organic solvent were purchased from Sigma-Aldrich.

The bacterial cultivation and protein purification processes were similar to those described in a previous report.[29] *Rhodobacter (Rba.) sphaeroides 2.4.1* cells were grown in M22+ medium at 30 °C under light for 3 days anaerobically and were harvested by centrifugation.

LH2 complex purification. The chromatophore was prepared by sonication and ultracentrifugation[30] and was successively resuspended and diluted in 20 mM Tris–HCl (pH 8.0) to $OD_{800} = 50\ cm^{-1}$. LDAO was added to a final concentration of 1% and stirred for 45 minutes under a nitrogen (N_2) atmosphere. The LH2 complex was then purified by anion-exchange column chromatography using DEAE-52. For spectroscopic measurement, the LH2 complex was eluted with TL buffer (0.1% LDAO, 20 mM Tris, pH 8.0).

Spheroidene preparation. All-*trans* spheroidene with conjugation C=C bond number 10 ($N = 10$) was extracted and purified from *Rba. sphaeroides 2.4.1* cells following a previous protocol.[31] A methanol-acetone mixture (2 : 7, v/v) was used to extract the pigment from wet cells several times. The obtained dry pigment mixture was dissolved in *n*-hexane and purified by Al_2O_3 column chromatography using a gradient *n*-hexane-diethyl ether mixture as the eluent. All-*trans*-spheroidene was recrystallized before further use in spectroscopic measurements.

Transient absorption spectroscopy

A commercial spectrometer (Helios Fire, Ultrafast System) is used to measure the femtosecond transient absorption spectra. A Ti:sapphire laser amplifier system (Astrella, Coherent, Inc., 35 fs, 7 W, 1 kHz) is used to produce the 800 nm fundamental beam. An actinic pump, which is at 480 nm for the experiment of spheroidene in *n*-hexane solution, 500 nm for the experiment of spheroidene in DMSO solution and 510 nm for the experiment of the LH2 complex, is generated using an optical parametric amplifier (OPerA Solo, Coherent, Inc.). The supercontinuum white light generated by focusing the 800 nm fundamental beam on a sapphire crystal plate worked as the probe pulse with a range from 470 to 640 nm. The instrument response function (IRF) of the system is ~120 fs.

Femtosecond stimulated Raman spectroscopy

We obtained a tunable narrowband picosecond (ps) Raman pump, a broadband femtosecond (fs) Raman probe, and an fs actinic pump by splitting the fundamental laser pulses (Coherent, Astrella, 35 fs, 7 mJ per pulse, 1 kHz repetition rate) into three. The actinic pump centered at 480/500/510 nm was generated using an optical parametric amplifier (OperA Solo, Coherent, Inc.). About 3 W of fundamental pulses were introduced into a second harmonic bandwidth compressor (SHBC, Coherent, Inc.) to produce ps 400 nm pulses and subsequently generate a ps Raman pump pulse through a ps-OPA system (TOPAS-400, Coherent, Inc.). The Raman pump wavelengths for Stokes excited-state Raman experiments for spheroidene in *n*-hexane solution are chosen as 530 nm, for spheroidene in DMSO solution and the LH2 complex are chosen as 550 nm, and for anti-Stokes experiments for spheroidene in *n*-hexane solution and the LH2 complex are chosen as 580 nm and 620 nm. Per pulse energy is about 150 nJ. About 15 mW of the fundamental laser output was focused onto a 2 mm thick single-crystal sapphire plate to generate the supercontinuum white Raman probe pulse. The spectral resolution of the FSRS setup was determined to be ~14 cm^{-1}, as estimated from the full width at half maximum (FWHM) of the narrowest ground-state Raman band (802 cm^{-1}) of cyclohexane measured under identical experimental conditions (see Fig. S1). The instrument response time was measured to be about 150 fs by cross correlation between the Raman probe pulses and fs actinic pump.

Results and discussion

The steady-state absorption spectra of the free spheroidene in *n*-hexane and DMSO and the LH2 complex are illustrated in Fig. 1a. The free spheroidene in *n*-hexane solution exhibits a characteristic $S_0 \rightarrow S_2$ (0–0) transition peak at 485 nm. Upon dissolution in DMSO solvent with higher polarizability, this absorption maximum undergoes a bathochromic shift to 503 nm.[32–35] A comparable redshift is observed in the LH2-bound spheroidene, where the 0–0 transition appears at 510 nm, indicating polarizability environment perturbation of the carotenoid's electronic structure.[35]

Fig. 1b–d compares the ground state FSRS spectra of the free spheroidene and LH2 complex. Three characteristic vibrational regions are identified: (1) The Raman modes at ~1520 cm^{-1} are assigned to the C=C stretching mode in the polyene chain. (2) The 1155 cm^{-1} feature arises from coupled C–C stretching and in-plane C–H bending modes. (3) Multiple peaks between 850 and 1000 cm^{-1} are diagnostic of C–H out-of-plane (HOOP) wagging vibrations. The detection of the HOOP modes in spheroidene indicates that there is distortion in the carotenoid backbone in its ground state.[36–39]

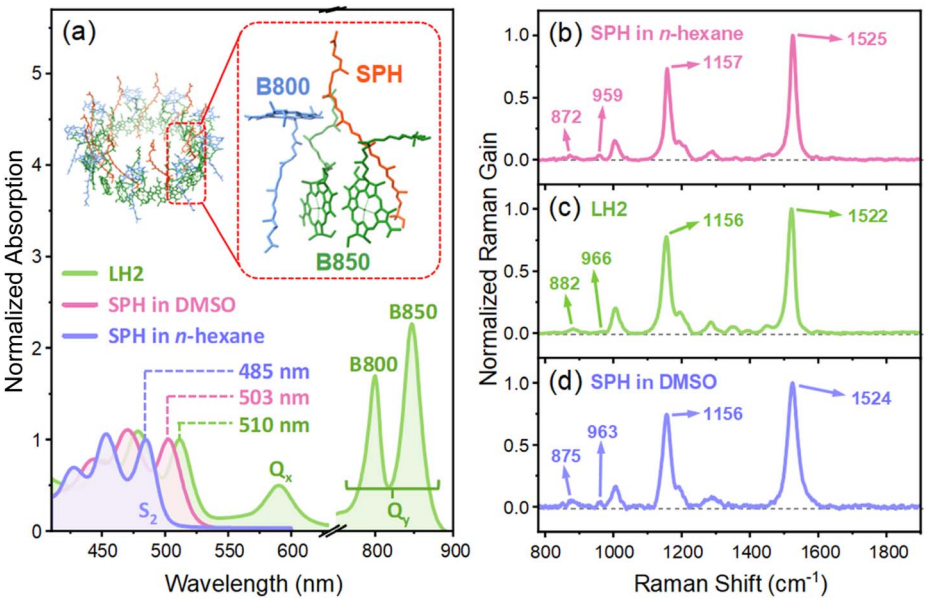

Fig. 1 (a) Steady-state absorption spectra of the LH2 complex and spheroidene (SPH) in DMSO and *n*-hexane solution; the inset shows the LH2 complex structure from *Rhodobacter sphaeroides 2.4.1.* (PDB:7PBW).[30] The ground state FSRS spectra of spheroidene in *n*-hexane (b), LH2 complex (c), and DMSO (d).

Excited-state structural dynamics are probed using FSRS with an actinic pulse energy of 150 nJ per pulse (Fig. 2–4, S5 and S6). To achieve the excited state Raman signal with a high signal to noise ratio, we employed Stokes-side FSRS (s-FSRS) using a 530 nm actinic pump for free spheroidene in *n*-hexane and a 550 nm for the LH2 complex and free spheroidene in DMSO (raw data are shown in Fig. S7). A Raman pump was used to obtain a high frequency (1000–2000 cm^{-1}) excited state Raman signal (green dashed lines labeled in Fig. S2). A strong transient absorption (TA) induced nonlinear background in the 100–1000 cm^{-1} range obscures the low-frequency Raman signal in s-FSRS. To overcome this, 580 nm (for free spheroidene in *n*-hexane) and 620 nm (for the LH2 complex and free spheroidene in DMSO) Raman pump wavelengths were selected for anti-Stokes-side FSRS (a-FSRS) to achieve pre-resonant enhancement of the low frequency range (100–1000 cm^{-1}) excited-state Raman signal (red dashed lines labeled in Fig. S2). These Raman pump wavelengths were selected to align with the excited-state absorption (ESA) bands and the stimulated emission (STE) band of the electronic excited states, based on the TA spectra shown in Fig. S2.

Fig. 2b shows the contour plot of 2D s-FSRS spectra of free spheroidene in the frequency range of 1650–1900 cm^{-1} in *n*-hexane, revealing a weak Raman mode at 1705 cm^{-1} and intense, broad Raman modes at ~1817 cm^{-1} that exhibit intricate rise and decay dynamics. The decay-associated difference spectra (DADS) extracted from global analysis is used to analyze the FSRS spectra, as shown in Fig. 2c. The DADS of the Raman modes in the frequency range of 1650–1900 cm^{-1} reveal complex dynamics; the three-time components ($\tau_1 = 150$ fs, $\tau_2 =$ 600 fs, and $\tau_3 = 8.5$ ps) from global fitting for these modes are consistent with the TA data obtained in the visible range (see Fig. S2). The Raman mode at 1705 cm^{-1} (red arrow in Fig. 2b) exhibits a single decay lifetime of $\tau_1 = 150$ fs, as shown in Fig. 2d, which signifies an ultrafast decay originating from the S_2 ($1B_u^+$) state. The detailed origin and assignment of this mode will be discussed later.

As depicted by dark blue arrows in Fig. 2b and the DADS in Fig. 2c, the s-FSRS reveals a two-stage evolution of Raman modes at ~1810 cm^{-1}: stage 1, the emergence of a Raman band at 1816 cm^{-1} within 150 fs (τ_1) that subsequently decays with a time constant of 600 fs (τ_2) and stage 2, the appearance of a new Raman mode at 1817 cm^{-1}, exhibiting an increase in intensity governed by τ_2 (600 fs), followed by a subsequent decrease with a time constant of $\tau_3 = 8.5$ ps.

As shown in Fig. S2b, the Raman pump wavelength was chosen to overlap with the ESA band of components τ_2 and τ_3 in TA spectra. Under these resonance conditions, the s-FSRS signals are dominated by the Raman gain signal with a Lorentzian line shape without noticeable dispersive distortion.[40,41] Consequently, both the transient Raman frequencies and amplitudes extracted from the two-stage Raman modes reliably reflect the underlying vibrational dynamics, allowing comparison of peak positions and their temporal evolution.

The transient Raman mode (1817 cm^{-1}) in stage 2, previously attributed to the in-phase C=C stretching mode of the optically forbidden S_1 ($2A_g^-$) state, arises from the vibronic coupling between S_1 ($2A_g^-$) and S_0 ($1A_g^-$) states.[17,24,25] According to the C_{2h} point group symmetry of all-*trans* polyenes, this coupling results in a frequency upshift to ~1817 cm^{-1} for the in-phase C=C stretching mode in the $2A_g^-$ excited state while simultaneously downshifting the corresponding mode frequency (1525 cm^{-1}) in the $1A_g^-$ ground state (Fig. 1b).[25,42,43] As shown in Fig. 2f, analysis of the transient amplitude of the

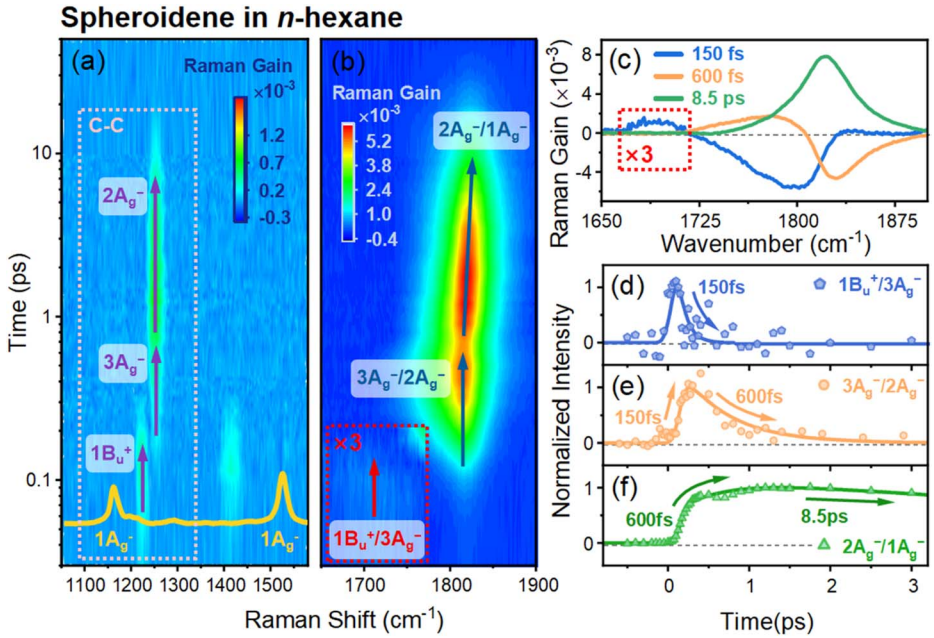

Fig. 2 The 2D contour plots of the s-FSRS signals from free spheroidene in *n*-hexane in the frequency range of (a) 1050–1580 cm^{-1} and (b) 1650–1900 cm^{-1}. (c) DADS of s-FSRS spectra in the Raman frequency range of 1650–1900 cm^{-1}. Transient kinetic traces of (d) $1B_u^+/3A_g^-$ diabatic mixing Raman mode at 1705 cm^{-1}, (e) $3A_g^-/2A_g^-$ vibronic coupling mode at 1740 cm^{-1}, and (f) $2A_g^-/1A_g^-$ vibronic coupling mode at 1817 cm^{-1}.

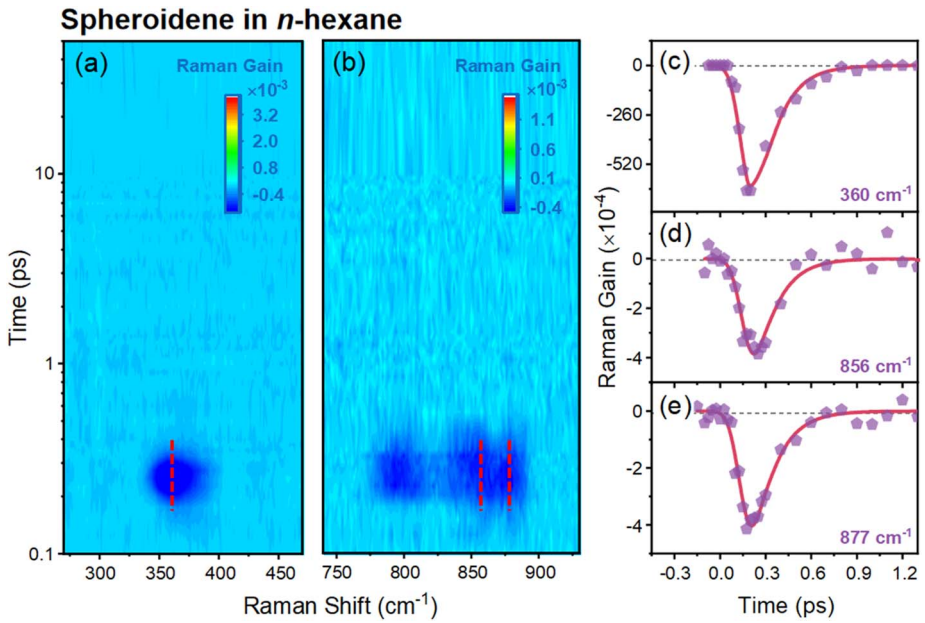

Fig. 3 The 2D contour plots of the a-FSRS signals from free spheroidene in *n*-hexane in the frequency range of (a) 270–470 cm^{-1} and (b) 740–930 cm^{-1}. Transient kinetic traces of Raman mode at (c) 360 cm^{-1}, (d) 856 cm^{-1}, and (e) 877 cm^{-1}.

Raman signal reveals a biphasic kinetic trace of this vibronic coupling mode: a slow rise dynamics (600 fs) followed by a decay with a lifetime of 8.5 ps. The 600 fs rise component is attributed to the population in a higher vibrational state in S_1 ($2A_g^-$) (hot S_1) from the upper excited state, accompanied by a vibrational cooling process. This population ultimately relaxes to S_0 ($1A_g^-$) states within 8.5 ps.[44] Notably, the vibrational mode undergoes a progressive blue shift during the $S_1 \rightarrow S_0$ internal conversion process (Fig. S3), a spectral shift directly correlating with the vibrational cooling dynamics in the S_1 ($2A_g^-$) state.[17]

In contrast to the S_1 dynamics, the temporal evolution of the Raman signal in stage 1 exhibits an initial ~150 fs rising

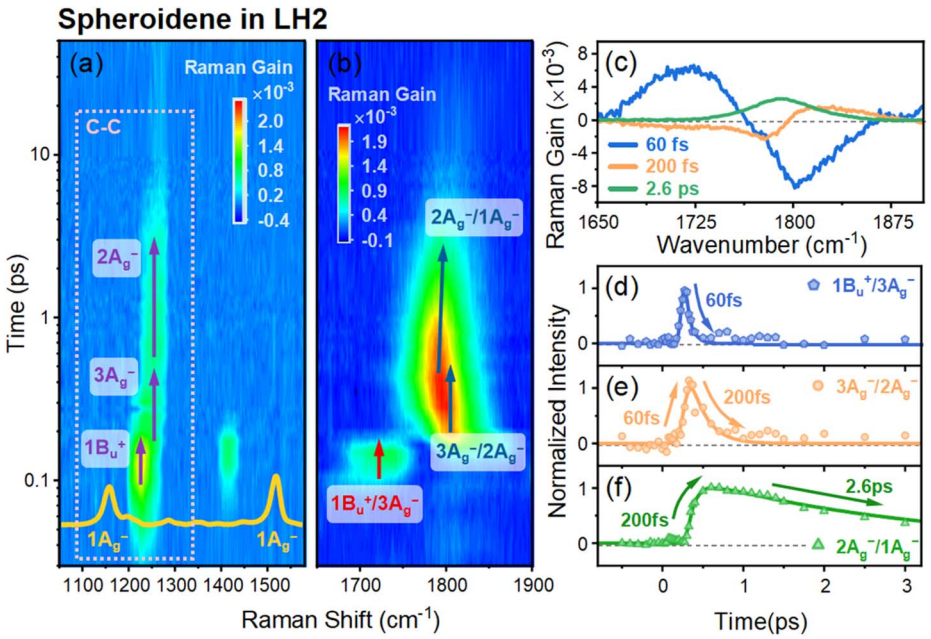

Fig. 4 The 2D contour plots of the s-FSRS signals from spheroidene in the LH2 complex in the frequency range of (a) 1050–1580 cm^{-1} and (b) 1650–1900 cm^{-1}. (c) DADS of s-FSRS spectra in the Raman frequency range of 1650–1900 cm^{-1}. Transient kinetic traces of (d) $1B_u^+/3A_g^-$ diabatic mixing Raman mode at 1721 cm^{-1}, (e) $3A_g^-/2A_g^-$ vibronic coupling mode at 1860 cm^{-1}, and (f) $2A_g^-/1A_g^-$ vibronic coupling mode at 1790 cm^{-1}.

dynamics followed by ~600 fs decay, as shown in Fig. 2e. The 150 fs rise coincides with the ultrafast depopulation of the S_2 ($1B_u^+$) state (Fig. 2d), indicating that the formation of the stage 1 Raman signal is directly correlated with the rapid S_2 relaxation process. The subsequent ~600 fs decay occurs on the same timescale as the ~600 fs rise observed for the S_1 ($2A_g^-$) state in stage 2 (Fig. 2f), suggesting a kinetic correspondence between the decay of the stage 1 signal and the build-up of the S_1 population in stage 2. This temporal correlation provides conclusive evidence for the existence of an intermediate state (S_X) mediating the S_2 ($1B_u^+$)-to-S_1 ($2A_g^-$) state transition, in comparison with the transient Raman signals of the S_2 and S_1 states in Fig. 2d and f. Notably, analogous to the $2A_g^-/1A_g^-$ vibronic coupling observed in stage 2, the detection of the unusually high frequency mode in stage 1 is indicative of vibronic coupling. Prior experimental and theoretical studies have characterized this intermediate (S_X) state as a discrete single excited state, with its symmetry assignment to $1B_u^-$[9–12] or A_g^+[16] configuration. However, our observation of a vibronic coupling mode rules out the A_g^+ assignment. According to the pseudo-parity selection rule, states with "−" Pariser labels cannot couple with "+" states *via* C=C stretching vibrations, and no vibronic coupling is expected between the $2A_g^-$ and $1B_u^+$ states or between the $2A_g^-$ and A_g^+[9,35] (unless the energy gap between "+" and "−" type states is very close to each other, which can induce a diabatic mixing[17,45]). Although the $1B_u^-$ state lies energetically between S_2 ($1B_u^+$) and S_1 ($2A_g^-$), fluorescence excitation spectroscopy studies have shown that internal conversion from $1B_u^-$ to $2A_g^-$ states is markedly inefficient,[46] suggesting that the $1B_u^-/2A_g^-$ vibronic coupling is symmetry-forbidden. In contrast, efficient internal conversion from $3A_g^-$ to $2A_g^-$ has been obtained, consistent with strong C=C vibronic coupling between these two states.[35] This agrees with our experimental results and supports assigning the stage 1 Raman mode (1816 cm^{-1}) to C=C vibronic coupling between $3A_g^-$ and $2A_g^-$ states.

In the ground state geometry of spheroidene, the $3A_g^-$ state lies above S_2 ($1B_u^+$) states.[13–15,28,44] Upon the vertical excitation to the S_2 ($1B_u^+$) state, however, energetic inversion may occur along the bond length alteration (BLA) coordinate[16,45] and polyene chain backbone distortion coordinate[17] near the S_2 potential energy minimum, where the $3A_g^-$ state acts as an intermediate state mediating the S_2 ($1B_u^+$)-to-S_1 ($2A_g^-$) state transition. This inversion highlights the critical role of geometric changes in modulating excited-state energy. A pronounced BLA decrease in excited states induces an increase in conjugated C=C bond length and a concomitant decrease in C–C bond lengths.[47] This structural reorganization directly impacts the vibrational spectrum, as evidenced by shifts in Raman-active modes.[47] In our experiment, as shown in Fig. 2a, an excited state Raman mode observed at 1223 cm^{-1} with a single decay lifetime of ~150 fs corresponds to the in-phase C–C stretching Raman mode, exhibiting a 66 cm^{-1} upshift in the S_2 ($1B_u^+$) state related to the S_0 ($1A_g^-$) state (1157 cm^{-1}).[48] This blueshift aligns with the BLA induced stiffening of the conjugated C–C bonds.[45,47] A further frequency upshift to 1252 cm^{-1} in S_X ($3A_g^-$) and S_1 ($2A_g^-$) states suggests additional C–C bond shortening (Fig. 2a), probably indicating a twisting dynamics in the S_2 ($1B_u^+$) state, leading to the formation of further structural distortion in the subsequent two dark ($3A_g^-$ and $2A_g^-$) excited states. In addition, a weak

transient Raman feature at around ~1400 cm^{-1} is observed with a single decay lifetime of ~150 fs. This mode is assigned to CH_3 symmetric deformation of the carotenoid methyl groups[38] and may be sensitive to initial photoinduced structural rearrangements of the polyene backbone or side groups. Support for this interpretation is provided by the appearance of enhanced low-frequency excited state Raman modes at less than 1000 cm^{-1} observed in a-FSRS by using a redder Raman pump at 550 nm. The a-FSRS spectrum reveals low-frequency Raman loss signals at 360 cm^{-1} (Fig. 3a and c), 780 cm^{-1}, 856 cm^{-1}, and 877 cm^{-1} (Fig. 3b, d and e), all exhibiting ~180 fs decay lifetimes, consistent with S_2 state dynamics. As demonstrated in prior anti-Stokes side FSRS studies, the Raman loss signal in the excited state is observed only when the wavelengths of the Raman pump and Raman probe are pre-resonant with the electronic transition of the STE band in the TA spectrum,[21,49] confirming selective probing of the optically bright S_2 ($1B_u^+$) state.

DFT calculations assign these modes to specific structural motions. The 360 cm^{-1} mode corresponds to polyene chain in-plane skeletal bending (Fig. S4a), while 856 cm^{-1} and 877 cm^{-1} modes are assigned to HOOP vibrations (Fig. S4b and c). Notably, carotenoid HOOP modes in 800–1000 cm^{-1} regimes exhibit exceptional sensitivity to restoring forces during chromophore twisting,[17,20] a phenomenon validated across biological and chemical systems *via* FSRS.[21,50,51] Collectively, these observations provide explicit evidence for spheroidene twisting during S_2 state evolution. This conformational change, combined with the BLA reducing $3A_g^-$ state energy, facilitates its emergence as an intermediate S_X state between S_2 ($1B_u^+$) and S_1 ($2A_g^-$) states.

To summarize our findings thus far, DADS of the FSRS for spheroidene demonstrate three decay components, indicating a four-state relaxation scheme $S_2(1B_u^+) \xrightarrow{150\ fs} S_x(3A_g^-) \xrightarrow{600\ fs} S_1(2A_g^-) \xrightarrow{8.5\ ps} S_0(1A_g^-)$. As proposed in the schematic diagram (Fig. 5a), the potential energy (PE) curves illustrate the photoreaction pathway driven by displacements along the BLA and twisting coordinates of C–C/C=C bonds. Following vertical excitation, the wavepacket on the S_2 ($1B_u^+$) state undergoes ultrafast relaxation and subsequently decays along these coordinates to populate a structurally distorted S_X ($3A_g^-$) state. Notably, the emergence of the 1705 cm^{-1} mode (red arrow in Fig. 2b) arises from concurrent BLA reduction and backbone distortion. These collective distortions induce energetic inversion between S_2 ($1B_u^+$) and S_X ($3A_g^-$) states, causing them to approach each other and form an exceptionally narrow energy gap during the inversion.[26,45] Consequently, this facilitates diabatic mixing between the S_2 ($1B_u^+$) and S_X ($3A_g^-$) states, leading to the observable modes at 1705 cm^{-1}.[17,26,45] The emergence of this mode corresponds to the instantaneous formation of the S_2 state, followed by 150 fs decay. This decay is synchronized with the population dynamics of the S_X ($3A_g^-$) state on the same time scale and is then followed by intramolecular conversion to the S_1 ($2A_g^-$) state within 600 fs. Finally, the S_1 population relaxes into a vibrationally hot, distorted S_0 ground state, which ultimately cools to regain the equilibrium all-*trans* S_0 configuration.[17]

To further elucidate how the protein environment modulates the structural dynamics of spheroidene, we performed FSRS measurements on the LH2 complex. Fig. 4a and b display the 2D s-FSRS spectra of the LH2 complex in the frequency range of 1000–1900 cm^{-1}. The protein-bound spheroidene pigment demonstrates analogous structural dynamics to that obtained from free spheroidene, as schematically illustrated in the PE diagram (Fig. 5a). Notably, as shown in Fig. 4b and c, the LH2 complex exhibits enhanced Raman-active mode at 1721 cm^{-1}, which is attributed to S_2 ($1B_u^+$)/S_X ($3A_g^-$) diabatic mixing. This mode originates from photon-induced structural distortions of

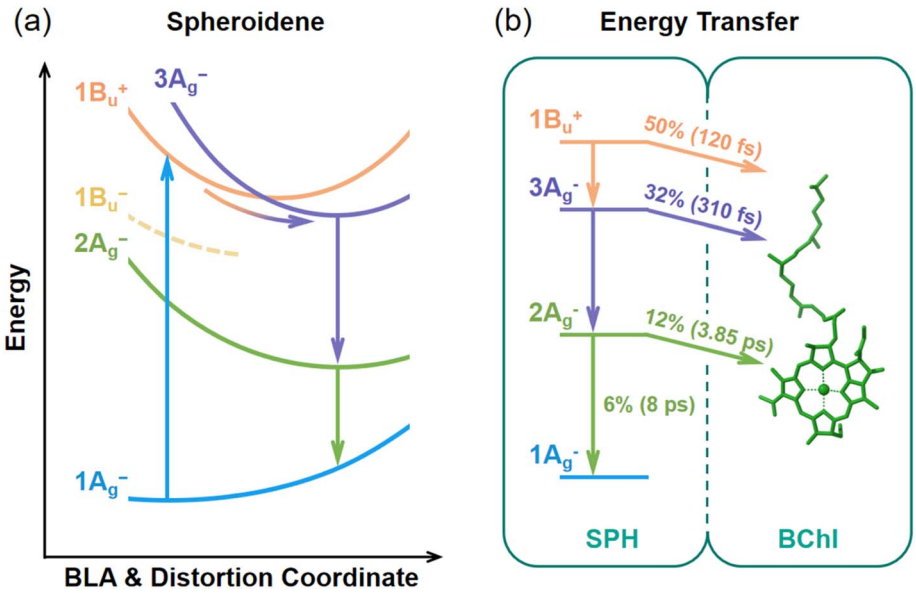

Fig. 5 Schematic diagrams depicting (a) the potential energy surface of spheroidene (SPH) along BLA and distortion coordinates of C–C/C=C bonds; (b) the excitation energy transfer quantum yield from spheroidene to BChl.

spheroidene in the LH2 complex that reduce the energy gap between S_2 ($1B_u^+$) and S_X ($3A_g^-$) during their inversion process. Supporting evidence includes (i) a blueshift excited-state C–C stretching mode at 1228 cm^{-1} *versus* its ground-state counterpart at 1156 cm^{-1} (Fig. 4a), reflecting BLA reduction and (ii) the activation of skeletal motion and HOOP modes at 358 and 885 cm^{-1} (Fig. S5), indicating backbone distortions. Importantly, the diabatic mixing signal of spheroidene is much more pronounced in LH2 than in *n*-hexane solution, highlighting the role of the protein environment in modulating the spheroidene's energy levels.[35,46]

As shown in Table 1, a comparative analysis of the $1B_u^+/3A_g^-$ C=C diabatic mixing mode undergoes a 16 cm^{-1} blue shift, while the $3A_g^-/2A_g^-$and $2A_g^-/1A_g^-$ vibronic coupling C=C stretching modes exhibit systematic redshifts of 6 cm^{-1} and 27 cm^{-1}, respectively, in the LH2 complex compared to free spheroidene in *n*-hexane. A similar downshifting trend is observed for ground-state $1A_g^-$ C=C stretching mode (Fig. 1b and c) and correlates with the redshift of the S_0 ($1A_g^-$) → S_2 ($1B_u^+$) electronic transition in steady absorption spectra (Fig. 1a). Together, these observations point to an enhanced environment polarizability within the protein binding pocket.[35,37,52]

Quantitatively, the average polarizability of spheroidene in the LH2 complex (R = 0.334) exceeds that in *n*-hexane (R = 0.23).[35,37] To further substantiate the role of environmental polarizability, spheroidene dissolved in DMSO (R = 0.28)[35] exhibits comparable frequency shifts (see Table 1). Relative to *n*-hexane, the $1B_u^+/3A_g^-$ C=C diabatic mixing mode blueshifts to 1711 cm^{-1} and $3A_g^-/2A_g^-$, $2A_g^-/1A_g^-$, and $1A_g^-$ related C=C vibronic coupling modes redshift to 1804 cm^{-1}, 1788 cm^{-1}, and 1524 cm^{-1}. In addition, an intensified $1B_u^+/3A_g^-$ diabatic mixing signature was observed at 1711 cm^{-1} (Fig. S6a and b). These results confirm that increased environmental polarizability plays a critical role in modulating the excited-state energy landscape of spheroidene.[37,46]

Comparative analysis of the DADS reveals distinct excited-state decay dynamics for spheroidene in different environments. However, the spheroidene demonstrates comparable triexponential decay components in both DMSO (τ_1 = 120 fs, τ_2 = 550 fs, and τ_3 = 8 ps) (Fig. S6b) and *n*-hexane solvents (τ_1 = 150 fs, τ_2 = 600 fs, and τ_3 = 8.5 ps) (Fig. 2c), indicating that solvent polarizability exerts only minor effects on the intrinsic excited-state relaxation pathways of spheroidene.[34,53] In sharp contrast, as shown in Fig. 4c, a remarkable acceleration of excited-state relaxation emerges within the LH2 complex, exhibiting significantly shortened lifetimes (τ_1 = 60 fs, τ_2 = 200 fs, and τ_3 = 2.6 ps), which are consistent with the TA results (Fig. S2c and d).[54] This significant decrease in spheroidene's S_2, S_X, and S_1 lifetimes, compared with their lifetimes in solutions, provides clear evidence for efficient spheroidene → BChl excitation energy transfer (EET).

To quantitatively evaluate these transfer processes, we calculate spheroidene → BChl EET lifetimes of S_2 ($\tau_{ET\text{-}1}$ = 120 fs), S_X ($\tau_{ET\text{-}2}$ = 310 fs), and S_1 ($\tau_{ET\text{-}3}$ = 3.85 ps) states, which are given by $\frac{1}{\tau_{LH2}} = \frac{1}{\tau_{ET}} + \frac{1}{\tau_{SPH}}$, where τ_{LH2} and τ_{SPH} are experimentally measured lifetimes of spheroidene in the LH2 complex ($\tau_{LH2\text{-}1}$ = 60 fs, $\tau_{LH2\text{-}2}$ = 200 fs, and $\tau_{LH2\text{-}3}$ = 2.6 ps) and in DMSO solution ($\tau_{SPH\text{-}1}$ = 120 fs, $\tau_{SPH\text{-}2}$ = 550 fs, and $\tau_{SPH\text{-}3}$ = 8 ps),[55,56] respectively. The energy transfer efficiencies (Φ_{ET}) are then determined from $\Phi_{ET} = \frac{\tau_{LH2}}{\tau_{ET}}$, yielding values of 50% for S_2, 64% for S_X, and 68% for S_1 states.

In addition to overall EET quantum yield of spheroidene to BChl, internal conversion between excited states needs to be considered. Specifically, 50% of the initial S_2 population undergoes internal conversion to the S_X state. The S_X state then transfers ~32% (50 × 64%) of the total energy to BChl, while the remaining ~18% (50 × 36%) is internally converted to the S_1 state. The S_1 state subsequently transfers ~12% (18 × 68%) of the total energy to BChl, with the remaining ~6% (18 × 32%) relaxing to the ground state S_0. Therefore, the total contributions of spheroidene to BChl energy transfer are quantified as 50% from S_2, 32% from S_X, and 12% from S_1, yielding an overall quantum yield (Φ_{ALL}) of 94% (Fig. 5b), in excellent agreement with previous experimental measurements.[4–7]

Theoretical studies suggest that structural distortion can break the C_{2h} symmetry of carotenoids, thereby enhancing coulombic coupling between the carotenoid S_1 ($2A_g^-$) and BChl (Q_y) states.[57] Consistent with this prediction, our FSRS results identify the dynamic structural distortion of spheroidene in its S_2 ($1B_u^+$) state, giving rise to distorted intermediate S_X ($3A_g^-$) and S_1 ($2A_g^-$) states. The involvement of such structurally distorted intermediates has been widely recognized in natural light-harvesting systems.[17,58–60] Photoexcitation of carotenoids induces subtle backbone twisting, which enhances coulombic coupling to nearby chlorophylls and facilitates carotenoid-to-chlorophyll energy transfer.[17] In our case, the structurally distorted intermediates of spheroidene may act as effective channels for ultrafast excitation energy delivery to BChls.

Table 1 The Raman peak positions for free spheroidene and spheroidene in the LH2 complex

	Spheroidene in *n*-hexane	Spheroidene in DMSO	LH2 complex
$1B_u^+/3A_g^-$	1705 cm^{-1}	1711 cm^{-1}	1721 cm^{-1}
$3A_g^-/2A_g^-$	1816 cm^{-1}	1804 cm^{-1}	1811 cm^{-1}
$2A_g^-/1A_g^-$	1817 cm^{-1}	1788 cm^{-1}	1790 cm^{-1}
$1A_g^-$	1525 cm^{-1}	1524 cm^{-1}	1522 cm^{-1}

Conclusions

In this work, we employed FSRS to directly observe photoinduced structural change of spheroidene in its S_2 ($1B_u^+$) state, leading to the formation of subsequent distorted S_X and S_1 ($2A_g^-$) intermediates. These results resolve the long-standing controversy regarding the S_X state: we show that BLA reduction and backbone twisting drive an energetic inversion between the $3A_g^-$ and S_2 ($1B_u^+$) states, thereby establishing a distorted S_X ($3A_g^-$) intermediate that mediates the S_2 ($1B_u^+$) → S_1 ($2A_g^-$) relaxation pathway. Quantitative analysis reveals spheroidene-to-BChl energy transfer efficiencies of 50% from S_2, 32% from

S_X, and 12% from S_1 states, yielding an overall efficiency of 94% in excellent agreement with previous reports. Photoinduced structural change not only activates the dark $3A_g^-$ state but may also enhance coulombic coupling between spheroidene and neighboring BChl molecules, thereby enabling ultrafast and highly efficient carotenoid-to-BChl energy transfer within the LH2 complex. By linking structural distortion with dark-state mediation, this study provides new insight into how photosynthetic light-harvesting systems exploit optically forbidden intermediate-state pathways to achieve remarkable transfer efficiencies.

Author contributions

B. P., M. C., and T. M. conceived, designed and performed the experiments. M. C. prepared the samples. B. P. and T. M. performed the experiments and analysed the experimental results. B. P., M. C., and T. M. co-wrote the manuscript. Y. H. did the DFT calculations. All authors participated in discussions and edited the manuscript. W. L. and P. W. directed the project.

Conflicts of interest

There are no conflicts to declare.

Data availability

Supplementary information (SI): cyclohexane ground-state FSRS; 2D TA spectra of spheroidene in *n*-hexane, DMSO, and LH2 complex; transient Raman frequency shift of the $3A_g^-$ mode of spheroidene in *n*-hexane; DFT calculation of spheroidene; 2D a-FSRS of spheroidene in LH2 complex; 2D s-FSRS of free spheroidene in DMSO. See DOI: https://doi.org/10.1039/d5sc08508j.

Acknowledgements

This work was supported by the National Natural Science Foundation of China (Nos. 22373068 and 22073112); the Double First-Class Initiative Fund of ShanghaiTech University; ShanghaiTech Start-up Funding (F-0201-16-006).

References

1 A. Telfer, A. Pascal and A. Gall, in *Carotenoids*, ed. G. Britton, S. Liaaen-Jensen and H. Pfander, Birkhäuser Basel, Basel, 2008, ch. 4, pp. 265–308.
2 Y.-Q. Li, Y.-H. Yan, R.-Y. Gao, J.-W. Zou, Y.-L. Wu, X.-Y. Yue, Y. Lu, X.-P. Wang, M.-Q. Chen, Q.-W. Li, H.-Y. Wang, P. Wang, L.-J. Yu, J. Zheng and J.-P. Zhang, Triplet excitation dynamics of photosynthetic light-harvesting antennae: mechanistic insights into the conjugation regulated carotenoid functionality, *Phys. Chem. Chem. Phys.*, 2025, **27**, 12462–12473.
3 J.-F. Hao, N. Yamano, C.-H. Qi, Y. Zhang, F. Ma, P. Wang, L.-J. Yu and J.-P. Zhang, Carotenoid-Mediated Long-Range Energy Transfer in the Light Harvesting–Reaction Center Complex from Photosynthetic Bacterium Roseiflexus castenholzii, *J. Phys. Chem. B*, 2023, **127**, 10360–10369.
4 P. J. Walla, P. A. Linden, C.-P. Hsu, G. D. Scholes and G. R. Fleming, Femtosecond dynamics of the forbidden carotenoid S1 state in light-harvesting complexes of purple bacteria observed after two-photon excitation, *Proc. Natl. Acad. Sci. U. S. A.*, 2000, **97**, 10808–10813.
5 H. Cong, D. M. Niedzwiedzki, G. N. Gibson, A. M. LaFountain, R. M. Kelsh, A. T. Gardiner, R. J. Cogdell and H. A. Frank, Ultrafast Time-Resolved Carotenoid to-Bacteriochlorophyll Energy Transfer in LH2 Complexes from Photosynthetic Bacteria, *J. Phys. Chem. B*, 2008, **112**, 10689–10703.
6 S. C. Chi, D. J. Mothersole, P. Dilbeck, D. M. Niedzwiedzki, H. Zhang, P. Qian, C. Vasilev, K. J. Grayson, P. J. Jackson, E. C. Martin, Y. Li, D. Holten and C. Neil Hunter, Assembly of functional photosystem complexes in Rhodobacter sphaeroides incorporating carotenoids from the spirilloxanthin pathway, *Biochim. Biophys. Acta Bioenerg.*, 2015, **1847**, 189–201.
7 J.-P. Zhang, T. Inaba, Y. Watanabe and Y. Koyama, Partition of carotenoid-to-bacteriochlorophyll singlet-energy transfer through two channels in the LH2 complex from Rhodobacter sphaeroides G1C, *Chem. Phys. Lett.*, 2001, **340**, 484–492.
8 E. Papagiannakis, J. T. M. Kennis, I. H. M. van Stokkum, R. J. Cogdell and R. van Grondelle, An alternative carotenoid-to-bacteriochlorophyll energy transfer pathway in photosynthetic light harvesting, *Proc. Natl. Acad. Sci. U. S. A.*, 2002, **99**, 6017–6022.
9 T. Sashima, H. Nagae, M. Kuki and Y. Koyama, A new singlet-excited state of all-trans-spheroidene as detected by resonance-Raman excitation profiles, *Chem. Phys. Lett.*, 1999, **299**, 187–194.
10 F. S. Rondonuwu, K. Yokoyama, R. Fujii, Y. Koyama, R. J. Cogdell and Y. Watanabe, The role of the $1^1B_u^-$ state in carotenoid-to-bacteriochlorophyll singlet-energy transfer in the LH2 antenna complexes from Rhodobacter sphaeroides G1C, Rhodobacter sphaeroides 2.4.1, Rhodospirillum molischianum and Rhodopseudomonas acidophila, *Chem. Phys. Lett.*, 2004, **390**, 314–322.
11 E. E. Ostroumov, R. M. Mulvaney, R. J. Cogdell and G. D. Scholes, Broadband 2D Electronic Spectroscopy Reveals a Carotenoid Dark State in Purple Bacteria, *Science*, 2013, **340**, 52–56.
12 E. Ostroumov, M. G. Müller, C. M. Marian, M. Kleinschmidt and A. R. Holzwarth, Electronic Coherence Provides a Direct Proof for Energy-Level Crossing in Photoexcited Lutein and β-Carotene, *Phys. Rev. Lett.*, 2009, **103**, 108302.
13 Y. Koyama, Y. Kakitani, T. Miki, R. Christiana and H. Nagae, Excited-State Dynamics of Overlapped Optically-Allowed $1B_u^+$ and Optically-Forbidden $1B_u^-$ or $3A_g^-$ Vibronic Levels of Carotenoids: Possible Roles in the Light-Harvesting Function, *Int. J. Mol. Sci.*, 2010, **11**, 1888–1929.
14 K. Furuichi, T. Sashima and Y. Koyama, The first detection of the $3A_g^-$ state in carotenoids using resonance-Raman excitation profiles, *Chem. Phys. Lett.*, 2002, **356**, 547–555.

15 Y. Koyama, F. S. Rondonuwu, R. Fujii and Y. Watanabe, Light-harvesting function of carotenoids in photosynthesis: The roles of the newly found $1^1B_u^-$ state, *Biopolymers*, 2004, **74**, 2–18.
16 J. Feng, C. W. Tseng, T. Chen, X. Leng, H. Yin, Y. C. Cheng, M. Rohlfing and Y. Ma, A new energy transfer channel from carotenoids to chlorophylls in purple bacteria, *Nat. Commun.*, 2017, **8**, 71.
17 T. Ma, M. Ruan, R. Zhao, Z. Wang, Y. Wang, Y. Huang, Y. Weng and W. Liu, Distorted Intermediate S_X ($1B_u^-$) State in Xanthophylls Drives Efficient Energy Transfer in Light-Harvesting Complex II, *J. Phys. Chem. Lett.*, 2025, **16**, 6711–6718.
18 Z. Wang, Y. Chen, J. Jiang, X. Zhao and W. Liu, Mapping photoisomerization dynamics on a three-state model potential energy surface in bacteriorhodopsin using femtosecond stimulated Raman spectroscopy, *Chem. Sci.*, 2025, **16**, 3713–3719.
19 P. G. Lynch, A. Das, S. Alam, C. C. Rich and R. R. Frontiera, Mastering Femtosecond Stimulated Raman Spectroscopy: A Practical Guide, *ACS Phys. Chem. Au*, 2024, **4**, 1–18.
20 B. Peng, Z. Wang, J. Jiang, Y. Huang and W. Liu, Investigation of ultrafast intermediate states during singlet fission in lycopene H-aggregate using femtosecond stimulated Raman spectroscopy, *J. Chem. Phys.*, 2024, **160**, 194304.
21 Y. Chen, Z. Wang, J. Jiang and W. Liu, Resolving Dual Photoreaction Channels of All-Trans-Retinal Using Femtosecond Stimulated Raman Spectroscopy, *J. Phys. Chem. B*, 2025, **129**, 7550–7556.
22 P. Kukura, D. W. McCamant and R. A. Mathies, Femtosecond Time-Resolved Stimulated Raman Spectroscopy of the S_2 ($1B_u^+$) Excited State of β-Carotene, *J. Phys. Chem. A*, 2004, **108**, 5921–5925.
23 S. Shim and R. A. Mathies, Development of a Tunable Femtosecond Stimulated Raman Apparatus and Its Application to β-Carotene, *J. Phys. Chem. B*, 2008, **112**, 4826–4832.
24 H. Hashimoto and Y. Koyama, The C=C stretching Raman lines of [β-carotene isomers in the S_1 state as detected by pump-probe resonance Raman spectroscopy, *Chem. Phys. Lett.*, 1989, **154**, 321–325.
25 H. Nagae, M. Kuki, J.-P. Zhang, T. Sashima, Y. Mukai and Y. Koyama, Vibronic Coupling through the In-Phase, C=C Stretching Mode Plays a Major Role in the $2A_g^-$ to $1A_g^-$ Internal Conversion of all-trans-β-Carotene, *J. Phys. Chem. A*, 2000, **104**, 4155–4166.
26 M. S. Marek, T. Buckup, J. Southall, R. J. Cogdell and M. Motzkus, Highlighting short-lived excited electronic states with pump-degenerate-four-wave-mixing, *J. Chem. Phys.*, 2013, 139.
27 T. Miki, T. Buckup, M. S. Krause, J. Southall, R. J. Cogdell and M. Motzkus, Vibronic coupling in the excited-states of carotenoids, *Phys. Chem. Chem. Phys.*, 2016, **18**, 11443–11453.
28 Y. Kakitani, T. Miki, Y. Koyama, H. Nagae, R. Nakamura and Y. Kanematsu, Vibrational relaxation and internal conversion in the overlapped optically-allowed $1B_u^+$ and optically-forbidden $1B_u^-$ or $3A_g^-$ vibronic levels of carotenoids: Effects of diabatic mixing as determined by Kerr-gate fluorescence spectroscopy, *Chem. Phys. Lett.*, 2009, **477**, 194–201.
29 D. M. Niedzwiedzki, C. N. Hunter and R. E. Blankenship, Evaluating the Nature of S_0-Called S*-State Feature in Transient Absorption of Carotenoids in Light-Harvesting Complex 2 (LH2) from Purple Photosynthetic Bacteria, *J. Phys. Chem. B*, 2016, **120**, 11123–11131.
30 P. Qian, D. J. K. Swainsbury, T. I. Croll, P. Castro-Hartmann, G. Divitini, K. Sader and C. N. Hunter, Cryo-EM Structure of the Rhodobacter sphaeroides Light-Harvesting 2 Complex at 2.1 Å, *Biochemistry*, 2021, **60**, 3302–3314.
31 T. Sashima, M. Shiba, H. Hashimoto, H. Nagae and Y. Koyama, The $2A_g^-$ energy of crystalline all-trans-spheroidene as determined by resonance-Raman excitation profiles, *Chem. Phys. Lett.*, 1998, **290**, 36–42.
32 M. Maiuri, D. Polli, D. Brida, L. Lüer, A. M. LaFountain, M. Fuciman, R. J. Cogdell, H. A. Frank and G. Cerullo, Solvent-dependent activation of intermediate excited states in the energy relaxation pathways of spheroidene, *Phys. Chem. Chem. Phys.*, 2012, **14**, 6312–6319.
33 P. O. Andersson, T. Gillbro, L. Ferguson and R. J. Cogdell, Absorption spectral shifts of carotenoids related to medium polarizability, *Photochem. Photobiol.*, 1991, **54**, 353–360.
34 A. N. Macpherson and T. Gillbro, Solvent Dependence of the Ultrafast S2−S1 Internal Conversion Rate of β-Carotene, *J. Phys. Chem. A*, 1998, **102**, 5049–5058.
35 M. Kuici, H. Nagae, R. J. Cogdell, K. Shimada and Y. Koyama, Solvent effect on spheroidene in nonpolar and polar solutions and the environment of spheroidene in the light-harvesting complexes of rhodobacter sphaeroides 2.4.1 as revealed by the energy of the $1A_g^- \rightarrow 1B_u^+$ absorption and the frequencies of the vibronically coupled C=C stretching raman lines in the $1A_g^-$ and $1B_u^-$ states, *Photochem. Photobiol.*, 1994, **59**, 116–124.
36 A. A. Pascal, Z. Liu, K. Broess, B. van Oort, H. van Amerongen, C. Wang, P. Horton, B. Robert, W. Chang and A. Ruban, Molecular basis of photoprotection and control of photosynthetic light-harvesting, *Nature*, 2005, **436**, 134–137.
37 M. J. Llansola-Portoles, A. A. Pascal and B. Robert, in *Methods in Enzymology*, ed. E. T. Wurtzel, Academic Press, 2022, vol. 674, ch. 4, pp. 113–135.
38 S. Saito and M. Tasumi, Normal-coordinate analysis of β-carotene isomers and assignments of the Raman and infrared bands, *J. Raman Spectrosc.*, 1983, **14**, 310–321.
39 J. Yu, L.-M. Fu, L.-J. Yu, Y. Shi, P. Wang, Z.-Y. Wang-Otomo and J.-P. Zhang, Carotenoid Singlet Fission Reactions in Bacterial Light Harvesting Complexes As Revealed by Triplet Excitation Profiles, *J. Am. Chem. Soc.*, 2017, **139**, 15984–15993.
40 S.-Y. Lee, D. Zhang, D. W. McCamant, P. Kukura and R. A. Mathies, Theory of femtosecond stimulated Raman spectroscopy, *J. Chem. Phys.*, 2004, **121**, 3632–3642.

41 K. Niu, B. Zhao, Z. Sun and S.-Y. Lee, Analysis of femtosecond stimulated Raman spectroscopy of excited-state evolution in bacteriorhodopsin, *J. Chem. Phys.*, 2010, **132**, 084510.

42 G. Orlandi, F. Zerbetto and M. Z. Zgierski, Theoretical analysis of spectra of short polyenes, *Chem. Rev.*, 1991, **91**, 867–891.

43 T. Noguchi, H. Hayashi, M. Tasumi and G. H. Atkinson, Solvent effects on the ag carbon-carbon double bond stretching mode in the $2^1A_g^-$ excited state of beta.-carotene and two derivatives: picosecond time-resolved resonance Raman spectroscopy, *J. Phys. Chem.*, 1991, **95**, 3167–3172.

44 F. S. Rondonuwu, Y. Watanabe, R. Fujii and Y. Koyama, A first detection of singlet to triplet conversion from the $1^1B_u^-$ to the 1^3A_g state and triplet internal conversion from the 1^3A_g to the 1^3B_u state in carotenoids: dependence on the conjugation length, *Chem. Phys. Lett.*, 2003, **376**, 292–301.

45 D. Accomasso, S. Arslancan, L. Cupellini, G. Granucci and B. Mennucci, Ultrafast Excited-State Dynamics of Carotenoids and the Role of the S_X State, *J. Phys. Chem. Lett.*, 2022, **13**, 6762–6769.

46 Y. Koyama, Y. Miki, T. Kameyama, R. J. Cogdell and Y. Watanabe, Low-lying electronic levels of spheroidene bound to the light-harvesting (LH2) complex of Rhodobacter sphaeroides 2.4.1 as determined by fluorescence and fluorescence—excitation spectroscopy at 170 K, *Chem. Phys. Lett.*, 1993, **208**, 479–485.

47 M. Jakučionis, I. Gaižiūnas, J. Šulskus and D. Abramavičius, Simulation of *Ab Initio* Optical Absorption Spectrum of β-Carotene with Fully Resolved S_0 and S_2 Vibrational Normal Modes, *J. Phys. Chem. A*, 2022, **126**, 180–189.

48 T. Noguchi, S. Kolaczkowski, C. Arbour, S. Aramaki, G. H. Atkinson, H. Hayashi and M. Tasumi, Resonance Raman spectrum of the excited $2A_g$ state of β-carotene, *Photochem. Photobiol.*, 1989, **50**, 603–609.

49 J. Wei, Y. Wu, R. Pu, L. Shi, J. Jiang, J. Du, Z. Guo, Y. Huang and W. Liu, Tracking Ultrafast Structural Dynamics in a Dual-Emission Anti-Kasha-Active Fluorophore Using Femtosecond Stimulated Raman Spectroscopy, *J. Phys. Chem. Lett.*, 2021, **12**, 4466–4473.

50 P. Kukura, D. W. McCamant, S. Yoon, D. B. Wandschneider and R. A. Mathies, Structural Observation of the Primary Isomerization in Vision with Femtosecond-Stimulated Raman, *Science*, 2005, **310**, 1006–1009.

51 C. Fang, R. R. Frontiera, R. Tran and R. A. Mathies, Mapping GFP structure evolution during proton transfer with femtosecond Raman spectroscopy, *Nature*, 2009, **462**, 200–204.

52 M. Macernis, J. Sulskus, S. Malickaja, B. Robert and L. Valkunas, Resonance Raman Spectra and Electronic Transitions in Carotenoids: A Density Functional Theory Study, *J. Phys. Chem. A*, 2014, **118**, 1817–1825.

53 H. A. Frank, J. A. Bautista, J. Josue, Z. Pendon, R. G. Hiller, F. P. Sharples, D. Gosztola and M. R. Wasielewski, Effect of the Solvent Environment on the Spectroscopic Properties and Dynamics of the Lowest Excited States of Carotenoids, *J. Phys. Chem. B*, 2000, **104**, 4569–4577.

54 M. Ricci, S. E. Bradforth, R. Jimenez and G. R. Fleming, Internal conversion and energy transfer dynamics of spheroidene in solution and in the LH-1 and LH-2 light-harvesting complexes, *Chem. Phys. Lett.*, 1996, **259**, 381–390.

55 E. E. Ostroumov, R. M. Mulvaney, J. M. Anna, R. J. Cogdell and G. D. Scholes, Energy transfer pathways in light-harvesting complexes of purple bacteria as revealed by global kinetic analysis of two-dimensional transient spectra, *J. Phys. Chem. B*, 2013, **117**, 11349–11362.

56 B. P. Krueger, G. D. Scholes and G. R. Fleming, Calculation of Couplings and Energy-Transfer Pathways between the Pigments of LH2 by the *ab Initio* Transition Density Cube Method, *J. Phys. Chem. B*, 1998, **102**, 5378–5386.

57 C.-P. Hsu, P. J. Walla, M. Head-Gordon and G. R. Fleming, The Role of the S_1 State of Carotenoids in Photosynthetic Energy Transfer: The Light-Harvesting Complex II of Purple Bacteria, *J. Phys. Chem. B*, 2001, **105**, 11016–11025.

58 T. Wei, V. Balevičius, T. Polívka, A. V. Ruban and C. D. P. Duffy, How carotenoid distortions may determine optical properties: lessons from the Orange Carotenoid Protein, *Phys. Chem. Chem. Phys.*, 2019, **21**, 23187–23197.

59 K. F. Fox, W. P. Bricker, C. Lo and C. D. P. Duffy, Distortions of the Xanthophylls Caused by Interactions with Neighboring Pigments and the LHCII Protein Are Crucial for Studying Energy Transfer Pathways within the Complex, *J. Phys. Chem. B*, 2015, **119**, 15550–15560.

60 S. Ghosh, J. D. Roscioli, M. M. Bishop, J. K. Gurchiek, A. M. LaFountain, H. A. Frank and W. F. Beck, Torsional Dynamics and Intramolecular Charge Transfer in the S_2 $(1^1B_u^+)$ Excited State of Peridinin: A Mechanism for Enhanced Mid-Visible Light Harvesting, *J. Phys. Chem. Lett.*, 2016, **7**, 3621–3626.